STATE RESEARCH CENTER OF RUSSIA
INSTITUTE FOR HIGH ENERGY PHYSICS
142281, Protvino, Moscow region, Russia

NuMI–NOTE–BEAM–1100

Design Study of the NuMI Target for 2 MW Upgrades

(Task A Report of the 2005 Accord between FNAL and IHEP)

V.Garkusha, A.Mikheyev*, I.Ponimash*, A.Ryabov,
T.Ryabova, F.Novoskoltsev, V.Zarucheisky

*) Institute of Physics and Power Engineering (IPPE), Obninsk, Kaluga reg., Russia

July 30, 2005

Contents

1 Outline

The present Report describes first results of the design study of the NuMI target for the 2 MW primary proton beam. This is in the view of Fermilab plans to use for neutrino experiments the proton beam with 5 times higher power with respect to the beam of the current accelerator complex (the Proton Driver project [1]). Two different Main Injector options, 120 GeV beam with 0.67 Hz cycle, and 40 GeV beam with 3 times higher repetition rate, were considered under the initial stage of the target study. In both cases the target should withstand the heat and mechanical load, created by the primary beam with 1.5×10^{14} protons per 8 μs pulse.

The water cooled target with a graphite core, encapsulated with prestress into the thin-walled metal pipe, has been examined as one possible variant of the target for the 2 MW primary proton beam. Similar designs, with graphite segments encapsulated into the stainless steel pipe, were considered early for the NuMI Low Energy target [2] and for the beam plug [3]. And lastly, $\sim$60 mm diameter graphite rods were encapsulated into the 1.5 mm thick aluminum pipe under construction of baffle collimators for the NuMI target hall [4].

Given below results were obtained without detailed optimizations of target and primary proton beam sizes. It was assumed that the primary proton beam on the target has the Gaussian distribution with $\sigma = 1.5$ mm in both transverse directions, and $r_0 = 5\sigma$. Here r_0 is the radius of a target core, and, at the same time, the radius of hole for a proton beam passing in the preceding baffle collimator.

Similar to the Low Energy target design, the ZXF-5Q graphite grade of Poco Graphite Inc. (see Appendix A) was chosen as a target core material for this stage of the design study.

2 Target Core Design

The target core consists of a row of 15 mm diameter and 30 mm length graphite cylinders, encapsulated with prestress into the stainless steel or aluminum thin-walled pipe. The target core is cut into segments in order to decrease thermal stresses. To avoid contact between heated segments, they are separated by $\sim$0.2 mm gaps. As will be shown below, an optimal (in the view of neutrino production) length of the target is about 1 m.

The internal volume of the target core is separated from an ambient air with help of two beam windows, and is blow out with a helium through small ventilating holes in each graphite segment.

Encapsulation of the graphite with prestress into the thin-walled pipe with help of the zone-normalized deformation method:

- provides an integrity of the target core, which consists of a row of separate segments, and keeps it even in the case of thermomechanical or radiation damages of some segments;
- prevents a direct contact of the cooling water with the heated surface of graphite, and, at the same time, provides a good thermal contact between the graphite and metal pipe.

Conceptual description of this method was given in our previous reports (see, for example, [2, 4]).

To a first approximation the value of prestress in case of the stainless steel pipe can be estimated as

$$P_0 \simeq (\alpha_p - \alpha_t) E \Delta T a / r_0,$$

where α_p and α_t are thermal expansion coefficients of pipe and target core materials, E and ΔT are the modulus of elasticity and the temperature inelastic limit of a pipe material, a is the pipe wall thickness. For the ZXF-5Q graphite and 16X12M2C2 stainless steel (Russian grade) $E \simeq 200$ GPa, $\Delta T \simeq 600^\circ$C, $\alpha_p - \alpha_t = 3 \times 10^{-6}$ K^{-1} the prestress $P_0 \simeq 10$ MPa.

Estimation of the prestress in case of the aluminum pipe can be made taking into account the plastic deformation only. The pressure, applied to the graphite, is

$$P_0 \simeq \frac{a}{r_0} \sigma_{02},$$

where σ_{02} is the yield strength of an aluminum alloy. For the aluminum pipe with $a = 1$ mm and $\sigma_{02} = 100$ MPa (Russian grade AMg2M) the prestress $P_0 \simeq 13$ MPa.

3 Energy Deposition in the Target Core

Calculations of an energy deposition were made using the IHEP version of MARS code [5] for two primary proton beam energies. As indicated above, distribution of the proton beam in transverse directions was taken as

$$N(r) = \frac{N_0}{2\pi\sigma^2} \exp(-\frac{r^2}{2\sigma^2})$$

with $N_0 = 1.5 \times 10^{14}$ protons per spill and $\sigma = 1.5$ mm.

Distributions along the target and numerical values of an energy, deposited by the 2 MW primary proton beam in the target core (graphite segments, encapsulated into a metal pipe), are given in terms of an average power in Figure 1 and Table 1. As it follows from these results:

- the power flux through the outer surface of target core reaches its peak of ~700 kW/m^2 at a depth of 20 cm for the 40 GeV primary beam, and ~600 kW/m^2 at the output of the 1 m length target for the 120 GeV beam. From this it follows, that in case of target cooling by means of the water forced convection, the heat transfer coefficient should be equal at least 15 kW/m^2/K in order to keep the time-average temperature of target reasonably below 100 ^{0}C;

- the maximal heat load on a metal pipe, surrounding the graphite, take place at the downstream end of target in case of the 120 GeV proton beam. Assuming that the heat capacity of stainless steel is about 0.5 kJ/kg/K, one would expect at this point of pipe the 180 ^{0}C temperature rise after the beam spill. For an aluminum pipe with the heat capacity of 0.9 kJ/kg/K the temperature rise is equal to 70 ^{0}C;

- for different primary beam and target design options the total power deposition in the target core is in order of 25 kW. Similar calculations, which were made using the GEANT3/FLUKA code gave ~10% higher value of total energy deposition.

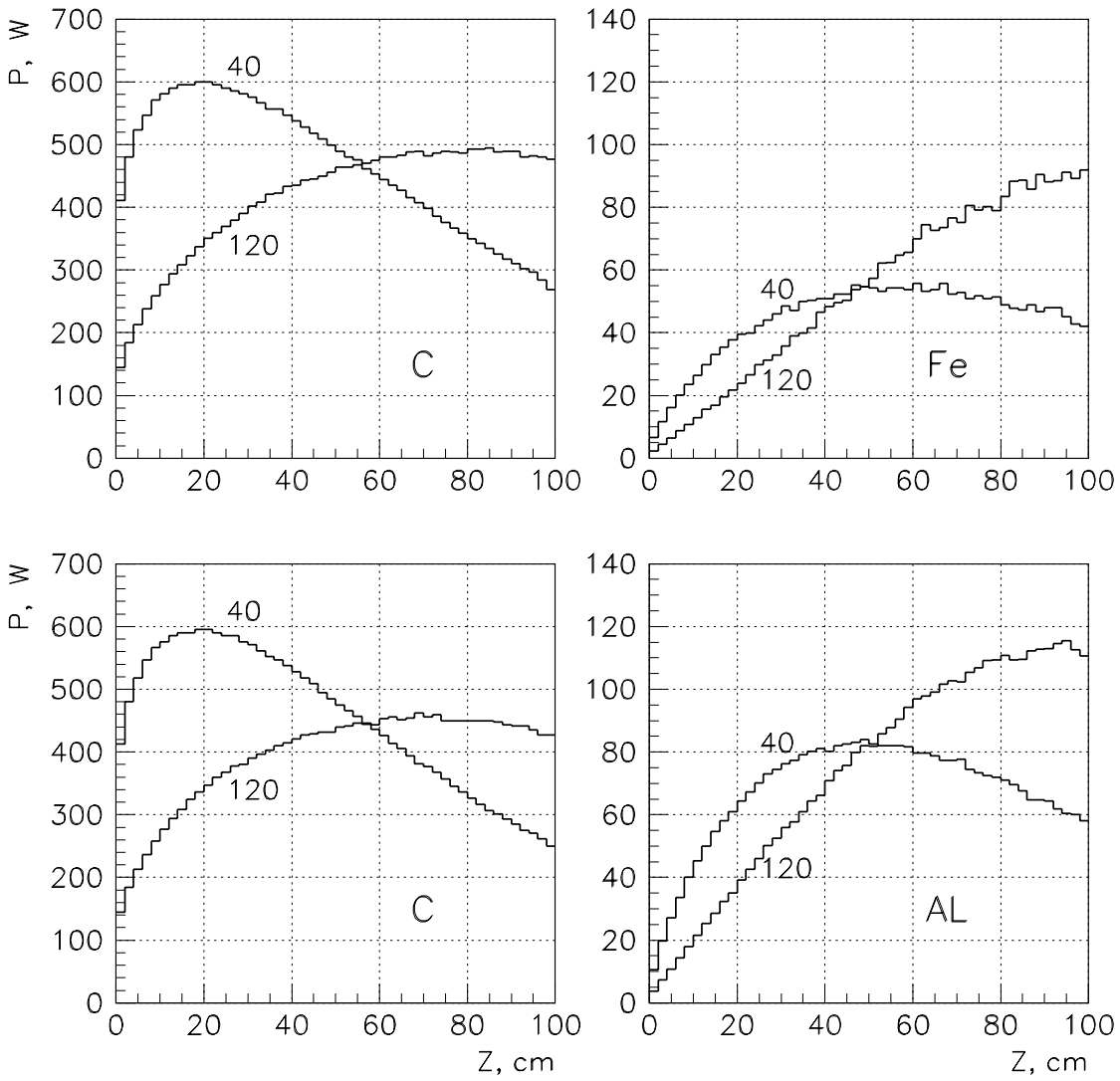

Figure 1: Distributions of an energy deposition along the target for two different primary proton beam energies. Top plots — for the graphite encapsulated in the 0.2 mm thick stainless steel pipe, bottom plots — for the graphite encapsulated in the 1 mm thick aluminum pipe.

Table 1: The total energy deposition (kW) in different parts of the 1 m length target.

Proton beam energy	40 GeV		120 GeV	
Graphite core	23.3	22.7	20.8	19.7
Steel pipe	2.2	—	2.7	—
Aluminum pipe	—	3.4	—	3.7
The whole target	25.5	26.1	23.5	23.4

4 Cooling of the Target

Cooling of the target by means of the water forced convection was considered in the first place. The cooling water passes through the 4 mm width co-axial channel, formed by the target core and the 0.3 mm thick stainless steel pipe. Taking into account power deposition in the cooling system itself, the total heat load to cooling system of the 1 m length target may be estimated by the value of 30 kW. Main parameters of the cooling system are summarized in Table 2. Calculations of the target temperature were made under the assumption that the inlet temperature of cooling water is equal to 37 ^{0}C.

Table 2: Main parameters of the water cooling system.

Velocity of a cooling water	2.2 m/sec
Heat transfer coefficient	15 kW/m^2/K
Water flow rate	30 l/min
Pressure drop	0.008 MPa
Outlet temperature of a water	52 ^{0}C

Temperature distributions along the target for two primary proton beam energies are shown in Figure 2. Following to profiles of energy depositions in the target core (see Figure 1), the water flow direction coincides with the beam direction for the 40 GeV option and is opposite to the beam direction for the 120 GeV one. Such choice of the water flow direction provides more flat temperature distribution along the target.

Energy deposition in a cooling water is responsible for the instantaneous temperature and, correspondingly, pressure rise, which values are related as

$$\Delta P = \frac{\beta \Delta T}{\kappa},$$

where β is the coefficient of volume expansion and $\kappa = 0.462 \times 10^{-9}$ 1/Pa is the volume compressibility. At the room temperature $\beta = 0.21 \times 10^{-3}$ 1/K and then increases with a temperature up to 0.77×10^{-3} 1/K at $T = 100$ ^{0}C.

Calculations show, that the instantaneous temperature rise in a cooling water reaches 20 ^{0}C at the downstream end of target in case of the 120 GeV primary beam[1]. For a cooling water with the temperature of 37 ^{0}C this

[1] In case of the 40 GeV beam the maximal value of temperature rise is approximately 1.5 times smaller.

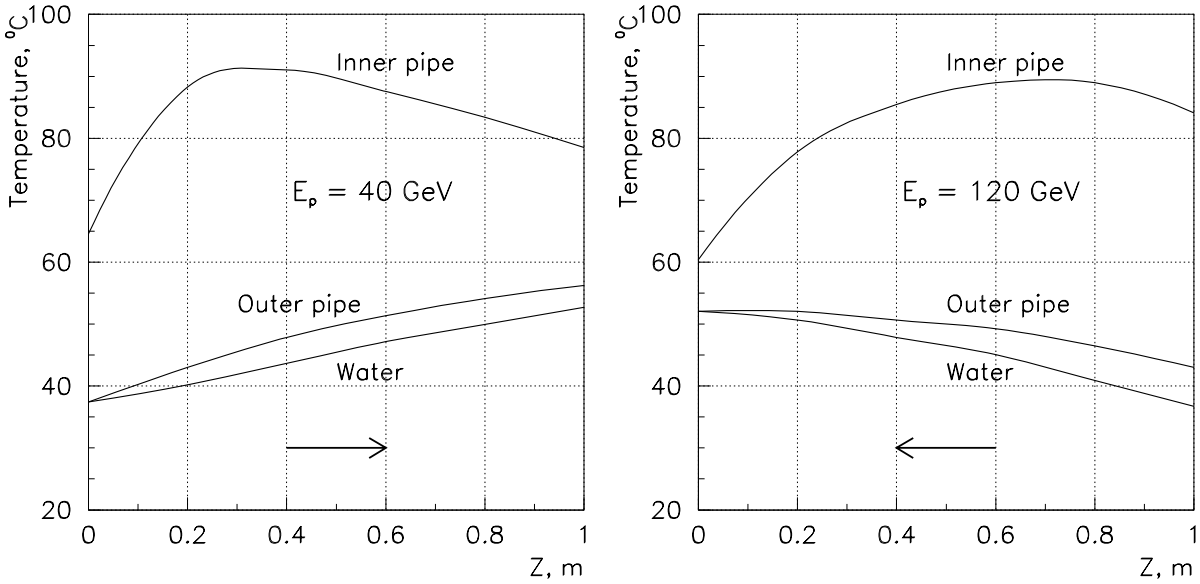

Figure 2: Temperature distributions in the cooling channel for two primary proton beam energies (water flow directions are shown with help of arrows).

results in the pressure jump of about 150 atm, which in case of the 8 μs beam spill may give rise to the failure of cooling system due to the hydraulic shock (water hammer).

Because of a temperature dependence of the volume expansion coefficient, the value of pressure rise may be reduced in a few times through the use of a cooling water with the temperature below 20 ^{0}C. However, the more effective way to avoid the failure of cooling system is a shock absorption by means of the two-phase water flow. That may be realized either by loading of the cooling water with He or Ar bubbles (10$\div$15% of volume), or by the use of boiling condition in the cooling channel.

In addition, it should be noted that the use of heat pipe shows considerable promise as a means for target cooling. The heat pipe is an enclosed system, which realizes a heat transfer from the hot zone to the refrigerator through evaporation and condensation of a working fluid (water). Water circulation is provided by the capillary-porous structure, covered the inside of heat pipe. Liquid and vapor phases are spatially divided in the heat pipe, what open up favorable conditions for stress relaxation in a water. To limitations of this method one can apply a complexity of construction and a relatively large temperature of target (up to 170 ^{0}C at the downstream end of target in case of the 120 GeV primary proton beam).

5 Results of Temperature and Stress Calculations

Calculations of temperature and stresses in target segments with the highest energy deposition density (EDD) were carried out using ANSYS under the following conditions:

- target segments with $r_0 = 7.5$ mm and $l = 30$ mm are encapsulated into the 0.2 mm thick stainless steel pipe with the prestress of 10 MPa;
- the thermal resistance between target segments and the stainless steel pipe is equal to zero;
- the heat transfer coefficient to a water is equal to 15 kW/m^2/K.

Temperature dependencies of mechanical and thermophysical properties of the ZXF-5Q graphite grade were taken into account, as well.

Results of temperature calculations are given in Table 3. Due to the smaller EDD at the beam axis, the temperature rise and, as may be expected, stresses are somewhat smaller in case of the 40 GeV proton beam.

Table 3: Temperatures in target segments with the highest EDD.

Primary proton beam energy, GeV	40	120
Segment number	2	6
EDD at the beam axis, GeV/cm^3/proton	0.025	0.033
Temperature of a water (see Figure 2), °C	37	50
Temperature at the beam axis, °C		
before the beam spill	120	80
after the beam spill	380	430
Temperature rise at the beam axis, °C	260	350

At the single turn extraction of beam from the Main Injector with the $\tau = 8$ μs pulse duration, the value $v_s\tau$ is of the same order of magnitude as target segment sizes (here $v_s \simeq \sqrt{E/\rho}$=2.8 mm/μs is the sound velocity in the graphite). It means, that stresses, which arise in target segments due to the heat load of beam, are essentially dynamical.

Time evolution of principal stresses ($\sigma_1 \geq \sigma_2 \geq \sigma_3$) at four specific points of the target segment are shown in Figure 3 in case of the 120 GeV primary proton beam. Point $P0(0,0)$ corresponds to the center of segment,

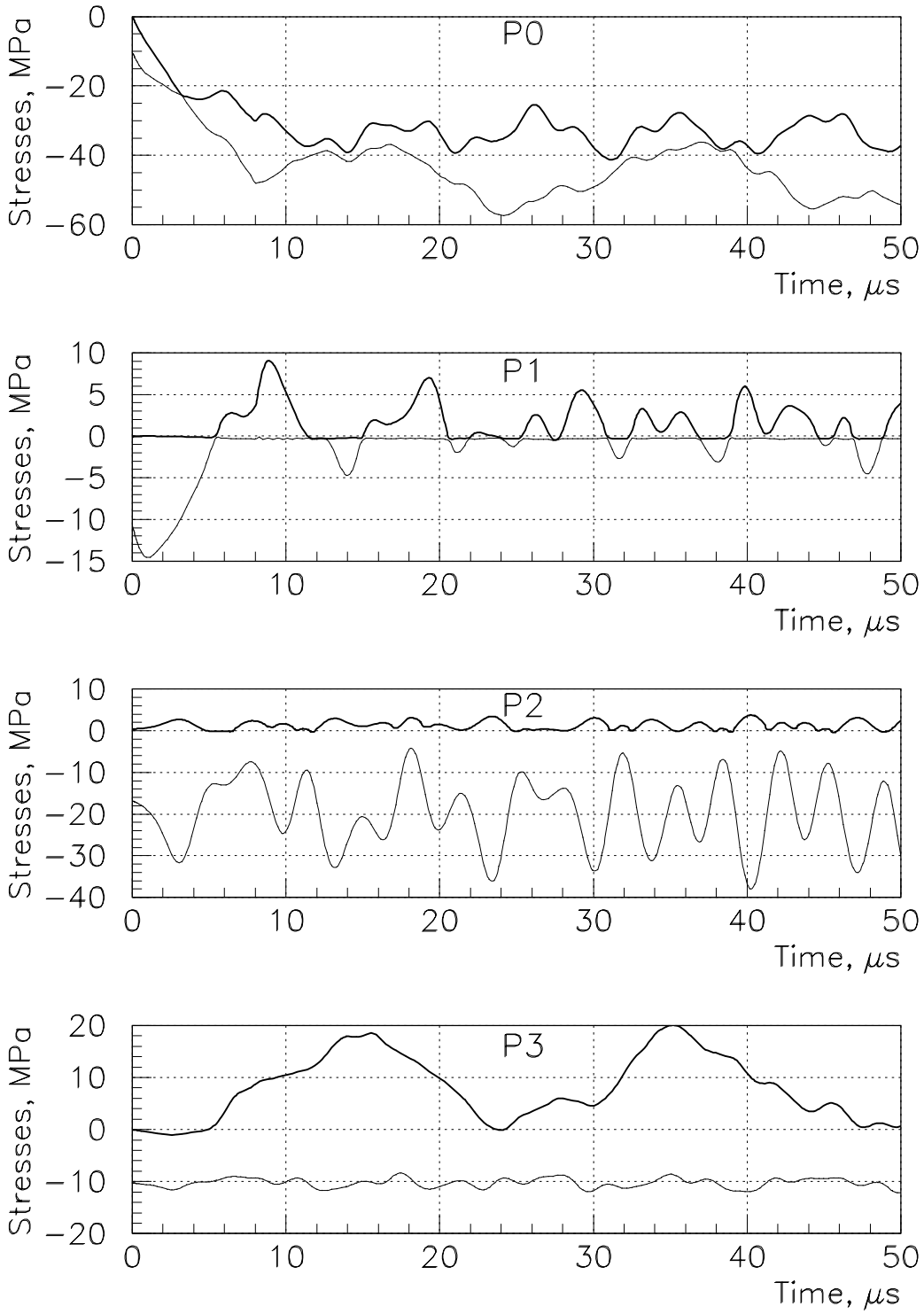

Figure 3: Time evolution of principal stresses σ_1 and σ_3 at some specific points of the target segment with the highest EDD in case of the 120 GeV primary proton beam. Point positions are given in the text.

$P1(0, l/2)$ is at the end surface of segment, $P2(r_0, l/2)$ and $P3(r_0, 0)$ are located at the lateral surface of segment.

As follows from these plots, the graphite is subjected to all-axis compression at point $P0$, while at points $P1 \div P3$ the stressed state has more complicated nature. The same behaviour of stresses take place in case of the 40 GeV primary proton beam too. Based on results of ANSYS calculations, safety margins for target segments were defined (see Table 4) with help of the Mohr-Coulomb criterion, taking into account the fatigue endurance limit for the graphite, as well.

The Mohr-Coulomb criterion is used mostly for brittle materials whose tensile and compressive properties are different. According to this criterion, which is based on the assumption that the principal stress σ_2 has a small effect on the marginal state and, therefore, can be neglected, the failure occurs when:

$$\begin{aligned} \sigma_1 \geq \sigma_t \qquad & \text{if} \qquad \sigma_1 > 0 \text{ and } \sigma_3 > 0, \\ -\sigma_3 \geq \sigma_c \qquad & \text{if} \qquad \sigma_1 < 0 \text{ and } \sigma_3 < 0, \\ \sigma_1/\sigma_t - \sigma_3/\sigma_c \geq 1 \qquad & \text{if} \qquad \sigma_1 \geq 0 \text{ and } \sigma_3 \leq 0, \end{aligned}$$

where σ_t and σ_c are tensile and compressive stress limits of the material.

Fatigue tests show that for 10^7 cycles, what corresponds to approximately one year of target operation, the fatigue endurance limit of graphite (the ratio of an applied stress to the first cycle strength) is in the range of 0.5-0.6 [6].

Table 4: Safety factors for different points of target segments with the highest EDD.

Beam energy, GeV	40	120
$P0(0, 0)$	2.3	1.9
$P1(0, l/2)$	7.5	5.5
$P2(r_0, l/2)$	2.7	2.3
$P3(r_0, 0)$	2.8	2.0

Data, given in Table 4 show that safety factors is quite reasonable for both proton beam energies. On the other hand, for the considered design of target core (with graphite segments, encapsulated into the stainless steel pipe), the survivability of target will not be lost even in case of the fatigue breakdown of graphite.

6 Target Windows

Another important feature of the considered target are two windows, which separate the target core from an ambient air, and prevent the leakage of helium used to blow up the internal volume of the target.

Calculations of a temperature in upstream and downstream windows were made on the assumption that the energy, deposited in a window, is evacuated through the rim surface of the window only. The heat transfer coefficient (HTC) to an ambient medium with the temperature of 20 ^{0}C was taken equal at least to 2 kW/m^2/K. Steady-state temperature distribution in the window was obtained as a solution of the heat conduction equation taking into account the temperature dependence of the specific heat.

The quasi-static radial and tangential stresses, induced due to non-uniform temperature distribution in the radially constrained disk, were calculated using the following formulas [7]

$$\sigma_r(r) = -\alpha E \left[\frac{1}{r^2} \int_0^r T(r) r dr + \frac{1+\nu}{1-\nu} \frac{1}{R^2} \int_0^R T(r) r dr \right],$$

$$\sigma_\varphi(r) = -\alpha E \left[T(r) - \frac{1}{r^2} \int_0^r T(r) r dr + \frac{1+\nu}{1-\nu} \frac{1}{R^2} \int_0^R T(r) r dr \right],$$

where R is the radius of the window; α, E and ν are the thermal expantion coefficient, the modulus of elasticity and the Poisson ratio of the window material. In the center of disk (at the beam axis) the window material is compressed with $|\sigma_r| = |\sigma_\varphi| = \sigma_{max}$.

6.1 Upstream window

Since the energy deposition in the upstream window is largely defined by ionization losses of primary protons, temperature and stress in the center of window are in strong dependence on the beam spot size. Results of temperature and stress calculations for the most common used beryllium window are given in Table 5. It was suggested that the 0.5 mm thick window with $R = 7.5$ mm is made of the S-65C beryllium grade of Brush Wellman, Inc. (see Appendix A).

Taking into account that the high-cycle fatigue endurance limit of beryllium is equal to its yield strength (260 MPa), the minimal proton beam spot size may be about of $\sigma = 3.0$ mm. In order to obtain a possibility to

Table 5: Temperatures and stresses at the beam axis of the upstream beryllium window for the proton beam with the energy of 120 GeV (HTC = 2 kW/m^2/K).

Beam spot size (σ), mm	1.50	2.00	2.50	3.00
Temperature before beam spill, ^{0}C	65	64	64	62
Temperature rise, ^{0}C	135	79	52	37
Temperature after beam spill, ^{0}C	200	143	116	99
Maximal stress (σ_{max}), MPa	410	319	272	240

work with a smaller beam spot size, one should apply the more intensive cooling of the window. For example, if the heat transfer coefficient increases to 4 kW/m^2/K, the allowed value of the beam σ decreases up to 2.0 mm ($\sigma_{max} \simeq 240$ MPa). Further increase of the heat transfer coefficient gives no way for a noticeable decrease of the proton beam spot size.

In case of the 40 GeV primary proton beam the use of beryllium for the upstream window is unlikely due to three times higher average power, deposited in the window[2].

As an alternative to beryllium, the graphite may be considered as a window material for the considered target[3]. At the approximately equal energy deposition, the safety factor (resistance to thermal shock for these materials) may be expressed as

$$SF = \frac{\sigma_u C_p}{\alpha E},$$

where σ_u and C_p are the ultimate stress limit and the specific heat of the material. Taking as σ_u the yield strength for beryllium and the compressive strength for the graphite, one can obtain $SF_{Be} = 0.14$ and $SF_C = 1.2$.

Table 6 gives results of temperature and stress calculations for a few millimeter thick window made of the ZXF-5Q graphite. Cooling conditions are the same as for the beryllium window. One should note, that for the 40 GeV primary beam the maximal temperature in the center of window reaches the oxidation threshold of the used graphite grade. Although this take place as low as 10-20 ms after the beam spill at the 0.5 s beam repeti-

[2] At $\sigma = 3.0$ mm and HTC = 2 kW/m^2/K the steady-state temperature before the beam spill is about 130 ^{0}C, what results in ~490 MPa stress in the center of window.

[3] The inner volume of target will be filled with helium and don't need a high vacuum tightness.

Table 6: Temperatures and stresses at the beam axis of the upstream graphite window for the proton beam with the $\sigma = 1.5$ mm spot size (HTC = 2 kW/m^2/K).

Proton beam energy, GeV	40	120
Temperature before beam spill, ^{0}C	183	70
Temperature rise, ^{0}C	280	280
Temperature after beam spill, ^{0}C	463	350
S_{max}, MPa	42	26

tion rate, the temperature in the center of window may be reduced either due to some increase of the beam spot size, or with help of more intensive cooling of the window (for example, $T_{max} \simeq 370$ ^{0}C either at $\sigma = 2.0$ mm, or at HTC = 6 kW/m^2/K).

For both proton beam energies the maximal value of stress in the center of window, where the graphite is subjected to all-axis compression, is significantly smaller than compressive strength of the ZXF-5Q graphite even with regard of the fatigue endurance limit (0.5-0.6 for 10^7 cycles [6]).

Due to very fast heat load of the window material by the primary beam, the stress analysis can not be limited by quasi-static consideration only, first of all for graphite windows. The maximal dynamic stress, arising in the center of disk, may be estimated as [8]

$$\sigma_{max}^{dyn} \simeq \frac{2\sigma}{v_s \tau} \alpha E \Delta T,$$

where ΔT is the temperature rise in the center of window; v_s is the sound velocity in material and τ is the beam spill duration.

For the graphite with $v_s = 2.8$ mm/μs the maximal value of dynamic stress in the center of window is $\sigma_{max}^{dyn} \simeq 4.5$ MPa, what is at a level of 10-15% of the quasi-static stress. For the beryllium with $v_s = 13$ mm/μs this value is about 3% of the quasi-static stress.

6.2 Downstream window

In contrast to the upstream window, temperature and stress in the downstream window do not depend on the primary beam spot size, and are defined mostly by the cooling efficiency. For the 120 GeV primary beam,

with the almost 2 times higher average power, deposited in the graphite window in comparisson to the 40 GeV beam (see Figure 2.2), results of calculations show that at the HTC = 4 (6) kW/m^2/K the maximal temperature and stress at the center of window are equal to 315 (280) ^{0}C and 35 (30) MPa, respectively.

7 Estimation of the Radiation Damage in Graphite

A simplified approach, which excludes complicated computations, was used for an estimation of the radiation damage of the graphite core in the considered target. This approach includes:

- approximate calculations of the number of dpa (displacements per atom) in graphite segments irradiated by the high-energy proton beam;
- comparison of obtained results with data on the irradiation damage of graphite due to reactor neutrons (in the absence of similar data for high energy protons).

The number of displacements per atom in material is [9]

$$N = \int_{E_{min}}^{E_{max}} f(E)dE \int_{T_{min}}^{T_{max}} \sigma(E,T)\nu(T)dT, \qquad (1)$$

where $f(E)$ is the flux of irradiated particles, $\sigma(E,T)$ is the cross-section for a particle of energy E to produce the displaced atom with the energy T in the range dT, $T_{min} = E_d$ is the energy required to produce the displaced atom, T_{max} is the maximal energy which can be transferred to atoms by the incident particle of energy E, and $\nu(T)$ is the number of atomic displacements due to a knock-on primary displacement of energy T (a radiation damage function). In the low energy region $\nu(T)$ is the staircase function

$$\nu(T) = \begin{cases} 0, & T \le E_d \ , \\ 1, & E_d \le T \le 2E_d. \end{cases}$$

For computations of $\nu(T)$ at higher transferred energies it is conveniently to use an approximation [10]

$$\nu(T) = \frac{T}{2E_d}[1 + Kg(\varepsilon)]^{-1},$$

$$g(\varepsilon) = 3.4008\varepsilon^{1/6} + 0.40244\varepsilon^{3/4} + \varepsilon,$$

where $\varepsilon = T/E_l$, and for carbon $K = 0.12748$, $E_l = 5687$ eV, $E_d = 25$ eV. Function $\nu(T)$ has the maximal value of $E_l/(2E_dK) \sim 900$, which is reached even at $T \sim 1$ MeV (Figure 4).

Based on (1) the number of atomic displacements may be estimated as

$$\int_{E_{min}}^{E_{max}} f(E)\sigma_{el}(E)\nu(E)dE < N < \int_{E_{min}}^{E_{max}} f(E)\sigma_t(E)\nu(E)dE, \qquad (2)$$

where σ_{el} and σ_t are elastic and total cross-sections of carbon nucleus for irradiated particles. Distinction between lower and upper assessed values is negligible for low energy particles with $E \leq 10 - 30$ MeV, and reaches $\sim$3 for particles in the GeV-energy range.

For the 120 GeV primary beam with $I_{pp} = 1.9 \times 10^{21}$ protons per year the number of atomic displacements produced by the primary proton beam itself at the beam axis of the 1-st target segment was estimated assuming that the beam has the Gaussian distribution with $\sigma = 1.5$ mm. Taking $f(E)dE = I_{pp} \,/\, 2\pi\sigma^2 = 1.3 \times 10^{22}$ cm^{-2}, $\sigma_t = 330$ mb and $\nu = 900$ we obtain $N_1 \simeq 1.2 \div 3.9$ dpa/year.

Fluxes of all hadrons should be taken into account for calculation of the dpa damage rate in subsequent target segments. Figure 5 shows energy spectra of hadrons calculated by the GEANT3/FLUKA code in the central part of the target segment with the highest energy deposition density. The number of atomic displacements produced in the graphite by neutrons of all energies, and charged hadrons with $E \geq 30$ MeV was estimated using the expression (2) with $\sigma_{el}(E)$ and $\sigma_t(E)$ from [11, 12]. The expression (1) with the differential Coulomb cross-section was used to estimate the number of atomic displacements produced by charged hadrons with $E < 30$ MeV. As a result, the estimated number of atomic displacements, produced in the central part of the 9-th segment, is $N_9 \simeq 1.5 \div 5$ dpa/year.

It is well known that irradiation of the graphite with reactor neutrons leads to dimensional changes of considerable magnitude, as well as to changes of its thermophysical and mechanical properties. By way of example Figure 6 shows the neutron fluence dependence of some properties of the GR-280 graphite, used in Russian nuclear reactors RBMK [13]. For given graphite grade at the irradiation temperature 500-600 ^{0}C the critical value of neutron fluence is determined as 21×10^{21} n/cm^2, what accordingly to [10] may be set approximately equal to 21 dpa.

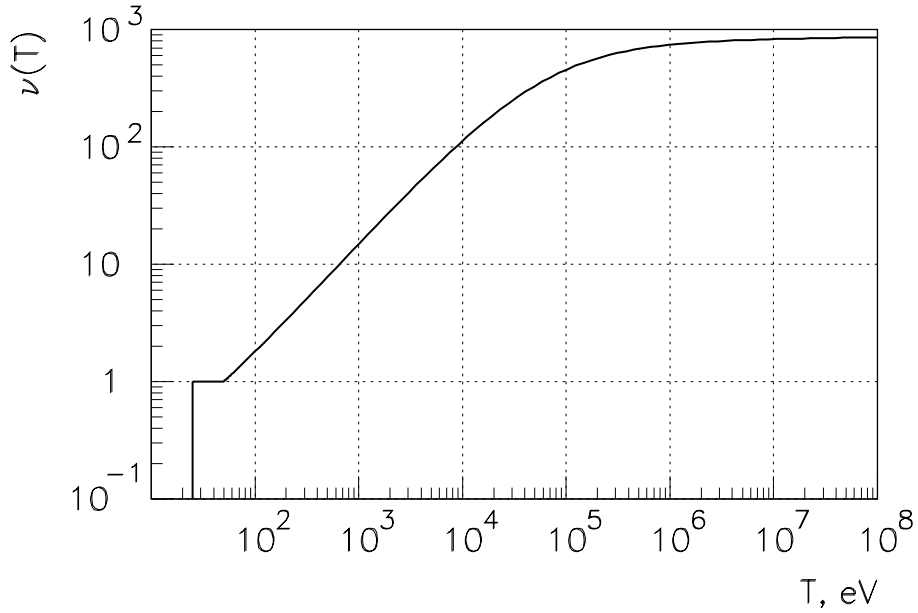

Figure 4: The number of atomic displacements $\nu(T)$ due to a primary displacement of energy T.

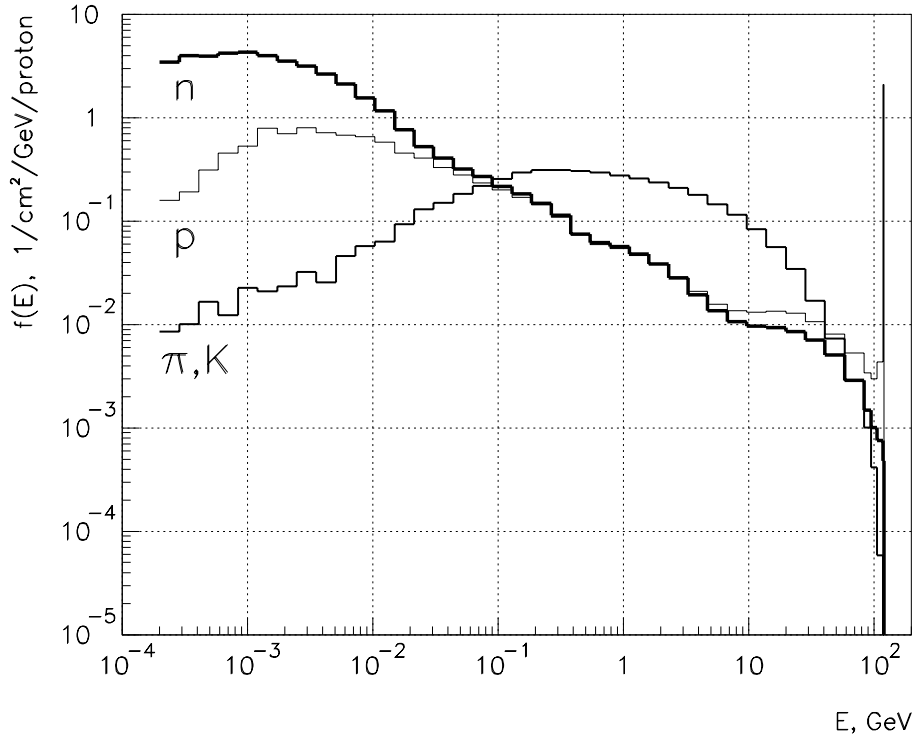

Figure 5: Energy spectra of hadrons at the beam axis of segment with the highest energy deposition density (9-th) in the case of the 120 GeV primary proton beam.

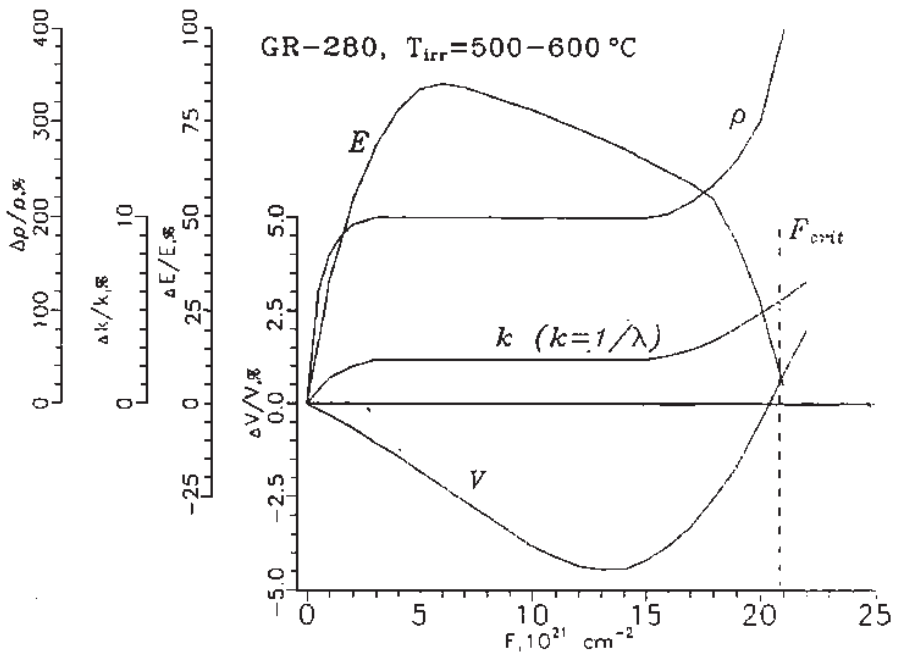

Figure 6: Determination of critical value of the neutron fluence for graphite, and changing of its physical properties under irradiation. V–volume; E–modulus of elasticity; k–thermal resistance; ρ–electrical resistance.

The lack of adequate information causes a lot of difficulties to determination of the critical value of neutron fluence for the Poco graphite grades, in particular ZXF-5Q one. Irradiation data presented in Figures 7 and 8 for AXF-8Q1 and AXZ-5Q1 Poco graphite grades[4] show, that in the range up to 5 dpa ($\simeq 5 \times 10^{21}$ n/cm^2), which corresponds to the radiation damage due to one year operation of the considered target with the 120 GeV primary proton beam:

- dimensional changes for these graphite grades seem as not very large;
- two times decrease of the thermal expansion coefficient will compensate approximately the same increase of the modulus of elasticity, keeping by this means the product of αE constant.

The last suggests, that stresses in the graphite due to heat load of the primary beam may remain invariable under irradiation of the target. On the other hand, the strength of graphite increases with irradiation to a

[4]Note, that these data are presented for relatively large irradiation temperatures with respect to the steady-state temperature of the target.

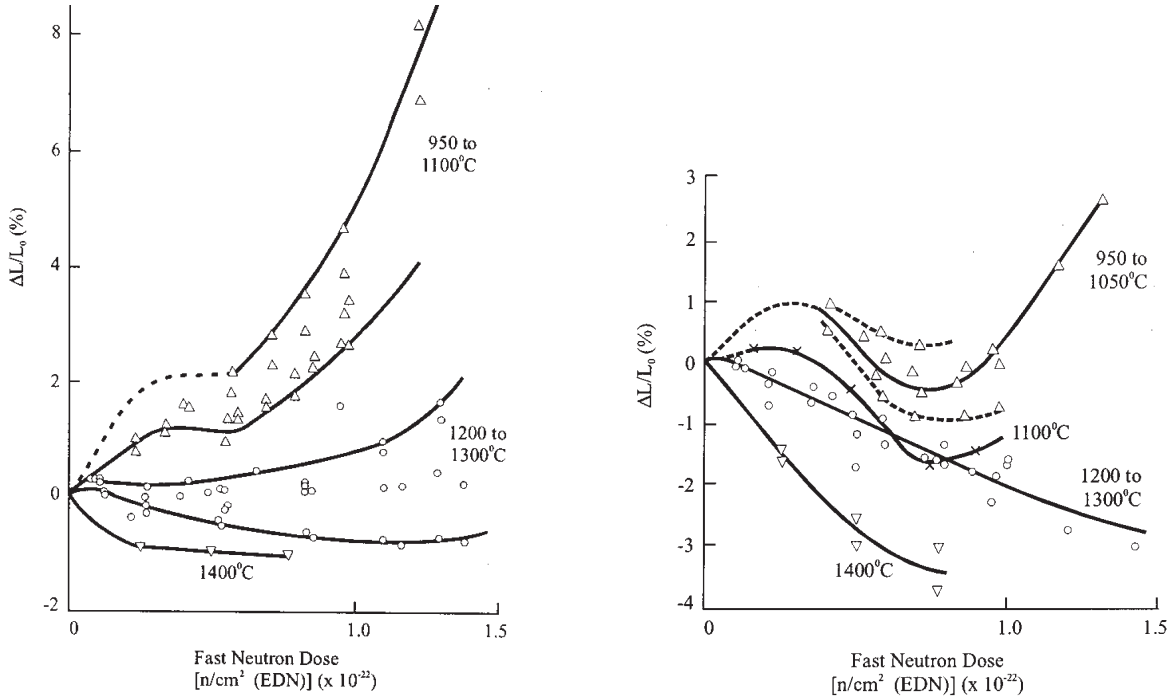

Figure 7: Dimensional changes of AXF-8Q1 (left) and AXZ-5Q1 (right) Poco graphite grades.

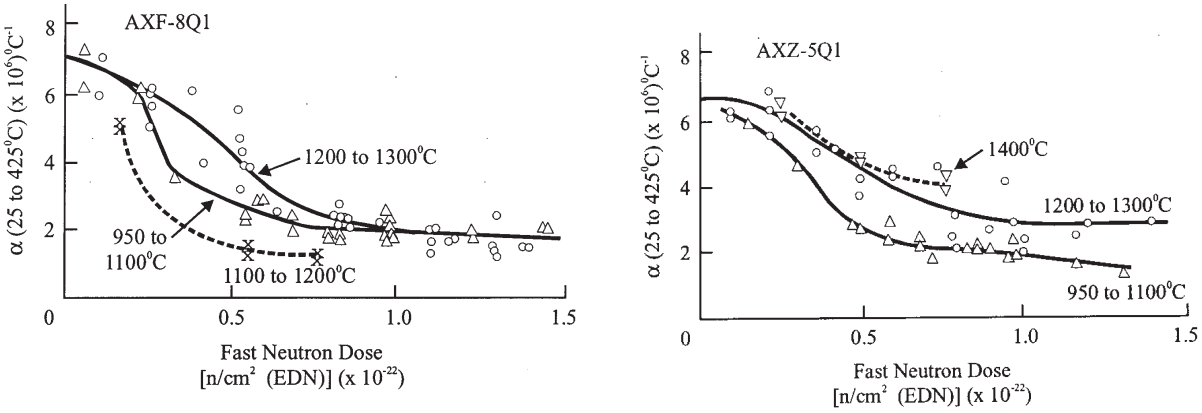

Figure 8: Variation of thermal expansion coefficients of AXF-8Q1 (left) and AXZ-5Q1 (right) Poco graphite grades.

point where the properties decline due to large structural effects [10]. Up to this point the strength in tension and shear increases according to

$$\sigma \geq \sigma_0 \sqrt{E/E_0},$$

where σ_0 is the unirradiated strength in the same direction and mode, E and E_0 are irradiated and unirradiated values of the modulus of elasticity.

To a good approximation the number of atomic displacements due to the 40 GeV primary beam with $I_{pp} = 5.7 \times 10^{21}$ protons per year is 3 times higher than that for the 120 GeV beam, and tends to the critical value of the dpa damage.

8 CC ν_μ Event Rates

Neutrino spectra, showing the impact on the neutrino beam of the target, which can withstand the 5 times higher power beam of the Proton Driver relative to beam of the current FNAL accelerator complex, are given in Figure 9. Calculations were made[5] for the 14 mrad off-axis NuMI beam in its Medium Energy (ME) configuration, which looks as more preferable for off-axis detector experiments [14].

Contrary to the current Low Energy (LE) beam configuration, in case of the ME beam the target is located outside the first horn [15] that removes any restrictions on its transverse sizes. The length of the ME target is equal to 1.2 m at the lowered to 1.54 g/cm^3 average density of the graphite target core, while the considered target is about 1 m in length with the average density of target core only 2÷3% smaller that the nominal density of graphite.

As is evident from Figure 9, at the equal number of incident protons:

- due do extra losses of secondaries in target core and cooling system materials, the considered target, labeled here as "2 MW target", provides ∼10% smaller total neutrino event rate with respect to the ME target (left plots);
- lowering of the primary proton beam energy from 120 GeV up to 40 GeV results in exactly three times decrease of the total neutrino event rate (right plots).

[5] Method of calculations and used computer codes are described in Appendix B.

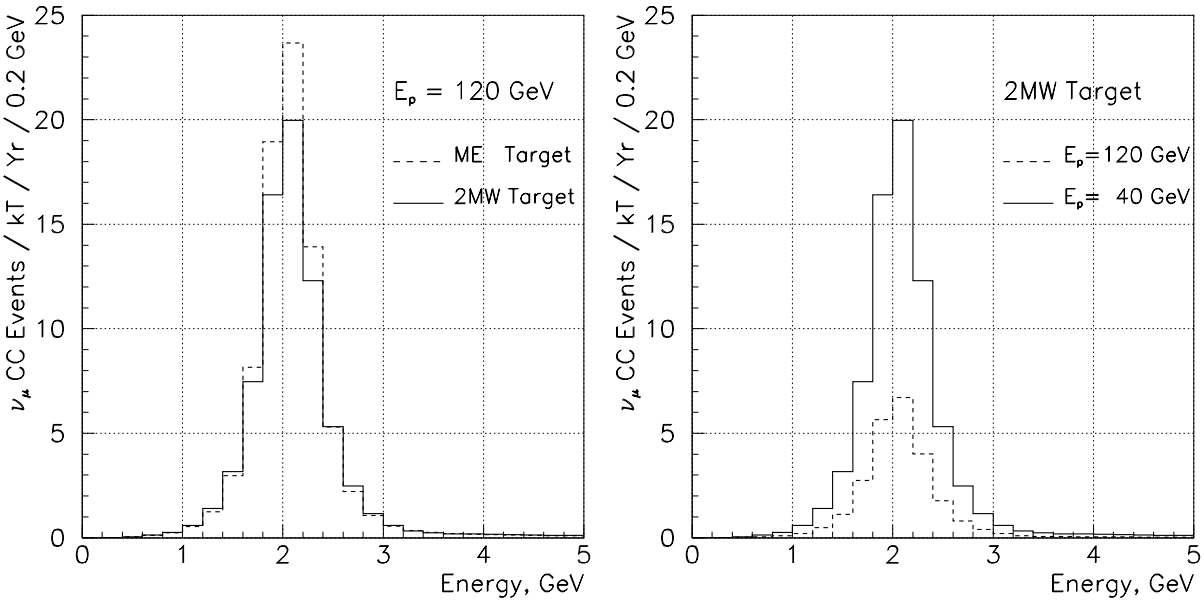

Figure 9: Neutrino event rates at the far detector for the 14 mrad off-axis NuMI beam (1 year = 3.8×10^{20} protons on the target).

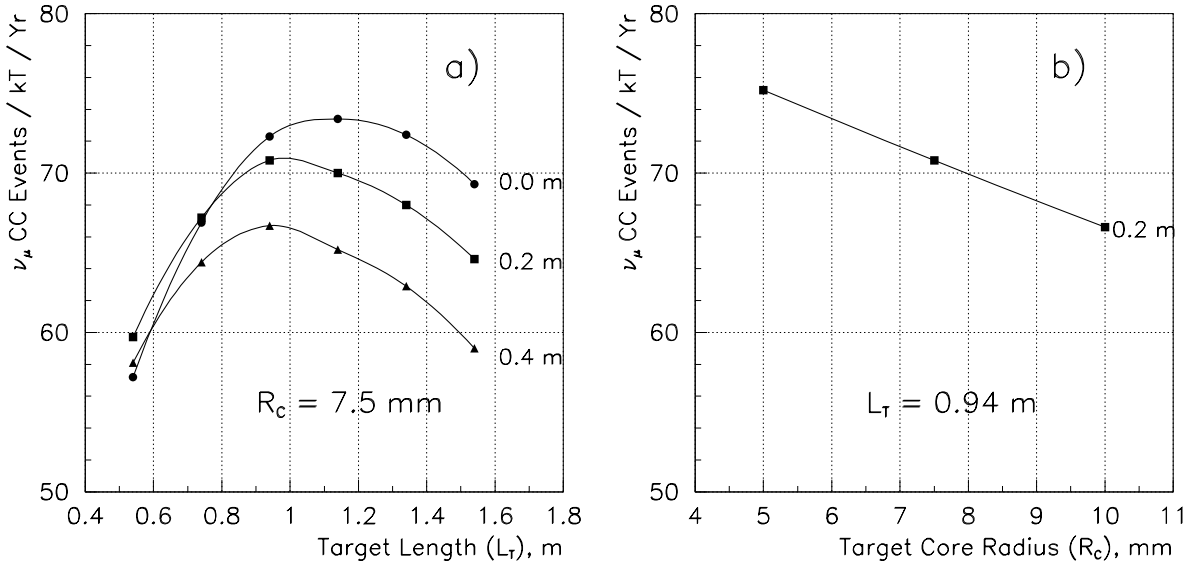

Figure 10: The total number of neutrino events at the far detector for the 14 mrad off-axis NuMI beam as functions of target length (a) and target core radius (b). The primary proton beam energy is equal to 120 GeV. Numbers near the plots give the values of gap between the target and the first horn.

Thus, in case of the 14 mrad off-axis NuMI beam, the use of a new target for the 2 MW proton beam of the Proton Driver could provide 4.5 times increase of the total neutrino event rate as compared with the ME target irradiated by the 0.4 MW proton beam of the current FNAL accelerator complex. Taking into account, that in case of the 40 GeV beam the total number of protons is 3 times higher, there is no difference between two considered primary proton beam energies from the point of view of neutrino production.

Given above results were obtained for the 0.94 m length new target, located 0.2 m upstream the first horn. This length is quite optimal in view of neutrino production for the 14 mrad off-axis NuMI beam, as follows from Figure 10a, which shows the total neutrino event rate at the far detector as a function of the target length at different values of the gap between target and horn. It is clear also, that the target should be located as close as possible to the first horn.

The dependence of the total neutrino event rate on the target core radius is given in Figure 10b. It can be seen, that a decrease of the target core (graphite) radius do not offer opportunities to increase substantially the number of neutrino events. Moreover, somewhat increase of the graphite radius is quite reasonable, because in this case we can increase the beam spot size and, as a result, reduce stresses without noticeable loss of the event rate.

9 Conclusions

Given above are results of preliminary design study for one possible variant of the target, which can withstand the 2 MW high energy proton beam with 1.5×10^{14} protons per pulse. The conducted study is sufficient to allow the following conclusions:

1. When constructed the considered target could provide 4.5 times increase of neutrino events for the 14 mrad off-axis NuMI beam, as the beam power increases from 0.4 MW of the current FNAL accelerator complex up to 2 MW of the Proton Driver.

2. The 120 GeV primary proton beam option appears more preferable than 40 GeV one, since at:

   - the equal total number of neutrino events at the far detector;
   - approximately the same energy deposition, temperatures and stresses in the target;

   for the 40 GeV primary beam, with 3 times higher repetition rate and the same number of protons per pulse, one should expect:

   - almost 3 times more radiation-induced defects in the target core;
   - 3 times higher power consumption for horns supply;
   - more than 2 times higher power deposition in horns (resistance and beam heat).

3. Cooling of target calls for further advanced study! Continuing the development of the water forced convection it is necessary to provide:

   - an estimation of the hydraulic shock impact on the cooling system;
   - an investigation of possibility to use the two-phase water flow for shock absorption.

   One should note, that the use of the heat pipe technology (evaporating cooling) shows considerable promise as one more possible variant of the two-phase cooling system for the 2 MW target.

   At the same time, it is appropriate to consider other possible variants of the target cooling, and, correspondingly, target design.

4. The use of graphite grades with the larger value of the thermal shock resistance $R = \sigma_t/\alpha E$ could provide at given primary beam spot size an increase of the safety factor for the target. For example, the R7650 graphite grade of SGL Carbon Group has $R = 0.66$ instead of $R \simeq 0.5$ for the considered at this stage of study the ZXF-5Q grade of Poco Inc.

Appendix A

Material Properties at 20 ^{0}C

Table A.1: Main properties of the ZXF-5Q graphite grade of Poco Graphite, Inc. [16].

Apparent density	1.81 g/cm^3
Compressive strength	195 MPa
Tensile strength	90 MPa
Modulus of elasticity	14.5×10^3 MPa
Poisson ratio	$\sim$0.2
Thermal conductivity	70 W/m/K
Coefficient of thermal expansion	8.1×10^{-6} 1/K
Specific heat	710 J/kg/K
Oxidation threshold	450 ^{0}C

Note: Oxidation threshold - the temperature that results in 1% weight loss in 24 hrs. No detectable reaction occurs at temperatures up to about 350 ^{0}C.

Table A.2: Main properties of the S-65C beryllium grade of Brush Wellman, Inc. [17].

Apparent density	1.82 g/cm^3
Ultimate tensile strength	370 MPa
Yield strength	260 MPa
Modulus of elasticity	310×10^3 MPa
Poisson ratio	$\sim$0.1
Thermal conductivity	200 W/m/K
Coefficient of thermal expansion	10.7×10^{-6} 1/K
Specific heat	1770 J/kg/K

Appendix B

Calculations of Neutrino Spectra

To obtain neutrino spectra without a large time consumption but, at the same time, with comprehensive simulation of the production target, neutrino event rates in the far detector have been calculated using the combination of two different computer codes.

Under this approach the GEANT3 package with FLUKA routines is used for calculations of pions (kaons) production in the target of arbitrary dimensions and materials. Resulting particles are picked up by modified version of HALO[6] and tracked through the focusing system and the decay pipe. Decay weights and detector acceptance for muon neutrinos are calculated at multiple locations along the focusing system and the decay pipe. Absorption and scattering of pions in the inner conductors of horns are taken into account, but tertiary particles are not generated.

Figure B.1 shows the neutrino spectrum, calculated by this means for the NuMI Low Energy beam, as compared with that, calculated with help of the GNuMI code, which was developed at Fermilab specifically for the NuMI beam design. As may be seen from these plots, the difference between two spectra does not exceed 10% in the energy range up to 6 GeV, what gives grounds to use the considered here approach for calculations of neutrino beam spectra.

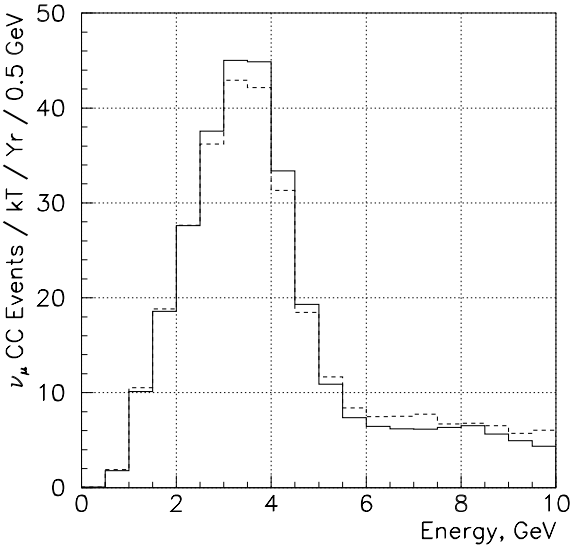

Figure B.1: The neutrino event rate at the far detector for the LE beam, calculated using GEANT3+HALO (solid line) and GNuMI (dashed line).

[6] This program, originally developed at CERN [18] for calculations of the muon background in charged particle beams, was modified to produce weighted neutrinos in the detector acceptance.

References

[1] W.Chou. Proton Driver for Super Neutrino Beam, Fermilab, March 25, 2004, http://www-bd.fnal.gov/pdriver/.

[2] P.Galkin, N.Galyaev, V.Garkusha et al. Comparison of Initial Conceptual Designs of the Low Energy Target, Protvino, 1999, NuMI-NOTE-GEN-0501.

[3] A.Abramov, V.Ferapontov, P.Galkin et al. Advanced Conceptual Design of the Low Energy Target and Beam Plug, Protvino, 1999, NuMI-NOTE-BEAM-0543.

[4] S.Filippov, V.Garkusha, R.Gibadullin et al. Technical Design of the Target Pile Protection Baffle, Protvino, 2002, NuMI-NOTE-BEAM-1092.

[5] I.Azhgirey, V.Talanov. MARS code status, Proceedings of XVII Workshop on Charged Particles Accelerators, v.2, p.184, Protvino, 2000.

[6] B.Wilkins. Journal of Materials 7(2), 251 (1972). B.Wilkins, A.Reich. AECL-4216 (1972).

[7] S.P.Timoshenko, J.N.Goodier. Theory of Elasticity, 2nd edition, "Science", Moscow, 1979.

[8] P.Sievers. Elastic Stress Waves due to Rapid Heating by an Intensive High-Energy Particle Beam, CERN LAB II/BT/74-2, Geneva, 1974.

[9] M.W.Thompson. Defects and Radiation Damage in Metals, Cambridge, The University Press, 1969.

[10] Irradiation Damage in Graphite due to Fast Neutrons in Fission and Fusion Systems, IAEA-TECDOC-1154, IAEA, Vienna, Austria, 2000.

[11] V.S.Barashenkov. Cross Sections for Interactions of Particles and Nuclei with Nuclei, JINR, Dubna, 1999.

[12] M.B.Chadwick, P.G.Young, R.E.MacFarlane, P.Moller, G.M.Hale, R.C.Little, A.J.Koning. LA150 Documentation of Cross Sections, Heating and Damage, Los Alamos National Laboratory Report LA-UR-99-1222, 1999.

[13] P.A.Platonov, O.K.Chugunov, V.N.Manevsky, V.I.Karpukhin. Radiation Damage and Life-time Evaluation of RBMK Graphite Stack, XA9642904, Russian Research Center Kurchatov Institute.

[14] NOvA. Proposal to Build a 30 Kiloton Off-Axis Detector to Study $\nu_\mu \to \nu_e$ Oscillations in the NuMI Beamline, March 21, 2005.

[15] A.G.Abramov, N.A.Galyaev, V.I.Garkusha et al. Beam Optics and Target Conceptual Designs for the NuMI Project, NIM, A485 (2002) 209.

[16] Poco Graphite Inc., A Unocal Company, 1601 South State Street, Decatur, Texas 76234.

[17] Brush Wellman Inc., Engineered Materials, 17876 St. Claire Avenue, Cleveland, Ohio 44110.

[18] Ch.Iselin, HALO. A Computer program to Calculate Muon Halo, Preprint CERN 74-17, 1974.